

Penetration of Human-Induced Warming into the World's Oceans

Tim P. Barnett,^{1*} David W. Pierce,¹ Krishna M. AchutaRao,² Peter J. Gleckler,² Benjamin D. Santer,² Jonathan M. Gregory,³ Warren M. Washington⁴

¹Climate Research Division, Scripps Institution of Oceanography, 0224, La Jolla, CA 92037, USA. ²Program for Climate Model Diagnoses and Intercomparison/Lawrence Livermore National Laboratory, Post Office Box 808, Livermore, CA 94550, USA.

³UK Met Office Hadley Centre and University of Reading, Reading RG6 6BB, UK. ⁴National Center for Atmospheric Research, Post Office Box 3000, Boulder, CO 80307, USA.

*To whom correspondence should be addressed. E-mail: tbarnett@ucsd.edu

A warming signal has penetrated into the world's oceans over the past 40 years. The signal is complex, with a vertical structure that varies widely by ocean; it cannot be explained by natural internal climate variability or solar and volcanic forcing, but is well simulated by two anthropogenically forced climate models. We conclude that it is of human origin, a conclusion robust to observational sampling and model differences. Changes in advection combine with surface forcing to give the overall warming pattern. The implications of this study suggest that society needs to seriously consider model predictions of future climate change.

Wide ranging evidence shows the earth has been warming in recent decades (1). Observations show approximately 84% of the total heating of the Earth system (oceans, atmosphere, continents, and cryosphere) over the last 40 years has gone into warming the oceans (2). Therefore if one wishes to understand and explain this warming, the oceans are clearly the place to look.

There have been only a few previous studies that have tried to both detect (i.e., differentiate from expected natural variability) and attribute (i.e., ascribe a cause to) the observed ocean warming signal (3–8). All used the equivalent of a single ocean basin temperature measure and tracked its change with time. This approach neglects information on how the warming penetrates vertically into the ocean, and variations of the penetration from basin to basin. The studies all suggest human impacts on the oceans, but some did not consider the possibility that the observed warming was due to natural external forcing such as solar variability or volcanic activity.

In this work we investigate the warming since 1960 on an ocean by ocean basis and pay special attention to how the signal penetrates down into the ocean. We use a recently upgraded and much expanded observed ocean data set (2), which provides the best available description of the ocean's warming signal and its evolution through time. In addition to examining this observational data, we compare it to

simulations from two independent climate models, the Parallel Climate Model (PCM) (9) and the Hadley Centre model (HadCM3) (10). We then use the results of numerical experiments with these models to attribute the causes of the observed warming. The models allow gross heat budgets to be constructed by basin; these show that changes in net surface heat flux conspire with advection at depth to give the observed signal.

We first define a model-based “fingerprint” describing the warming signal at each vertical level using the geographical and temporal variability of ocean temperature (11). The observations, projected on to this fingerprint at each level, show that the strength of the warming signal varies from ocean to ocean (12) (Fig. 1). The warming extends to depths of 700 m or more in both the N. and S. Atlantic, but is largely confined to the upper 100 m of the N. Pacific and N. Indian Oceans. The N. Indian Ocean is particularly unusual for it has a subsurface maximum. Both the N. and S. Pacific show a sign reversal in the warming signals, indicating a cooling around 150 m depth. These differences between oceans constitute the spatial structure of the warming fingerprint. The final dimension of the signal is the temporal evolution of the differences. Since we are interested in low frequency variations, we use decadal time averages to describe this time evolution.

Our purpose is to understand the origin of this complex time and space dependent signal. We explore three possible causes: natural variability internal to the coupled ocean-atmosphere system; external natural variability, such as solar or volcanic forcing; and forcing arising from human activity (emission of greenhouse gases and sulfate aerosols).

The likelihood that natural internal climate variability is the cause of the observed warming signal can be examined by analyzing a long control run of PCM; i.e., how well did natural internal variability in the control run project onto the warming fingerprint (12)? This approach was used in earlier work (3) and is a variant of standard detection and attribution analysis (13–16). It has the advantage of having a simple

geometric explanation while being rigorous in a statistical sense (17).

The strength of the warming signal in the control run (sampled in the same places as the observations) is shown in Fig. 2 for each ocean. This gives some indication of the fluctuations in signal strength that one might expect due to natural internal variability alone. Because we had multiple realizations of the 40 year time period in the control runs, we can show the 90% confidence limits of the natural variability by the hatched region. Also shown is the signal strength in the observations (red dots) from Fig. 1. The illustration leaves no doubt that the warming signal is far stronger than would be expected from natural internal variability, as estimated by the model. To see if the model's estimate of natural variability is reasonable, we compared the levels of variance in the control run at decadal time scales to those observed and found they matched reasonably well (18) (supporting online text). This means that the control run variations are a reasonable representation of natural internal variability, at least on the decadal time scales of interest here.

Another possible candidate for the warming signal is natural variability external to the ocean-atmosphere system, such as solar variability or volcanic eruptions ("SV" forcing). We explored this possibility by analyzing PCM runs forced by estimates of observed solar variability and volcanic aerosol loadings (19). The results of four such runs were combined and the warming signal strength estimated in the SV data set. The results (Fig. 2) show that in none of the oceans can the SV forcing (green triangles) replicate the observed warming. In fact, at these space and time scales the SV forcing produces signal strengths indistinguishable from those expected from natural internal variability (hatched region).

The final candidate for explaining the signal is anthropogenic factors, such as well-mixed greenhouse gases and sulfate aerosol particles. We examined this possibility in an ensemble of five PCM runs with such forcing (19, 20). The results (Fig. 3) show the range of the signal strength in five scenario runs by ocean and depth (hatched area) in comparison with the observations (red dots). An ocean by ocean and depth by depth comparison shows the agreement is compelling. The immediate conclusion is that human influences are largely responsible for the warming signal. This level of agreement could not have been tuned into the models, since the fingerprint is too complex in space and time. Further, about half of the observations used in this study were not available when the computer simulations were run. The different response of individual oceans to greenhouse gas (GHG) forcing is an interesting finding. The physical reasons for this are fairly well known, with one major surprise. For instance, it is well known that deep convection is characteristic of both the N. and S. Atlantic oceans (21). That

explains why the warming signal penetrates relatively deeply in these oceans. In contrast, the N. Pacific is characterized by a rather shallow meridional overturning circulation (22) that tends to isolate the surface layers from the deeper ocean. It is also true that no deep water is formed in the N. Pacific. Both physical properties act to confine the signal to the upper ocean. The same situation is thought to hold over much of the southern Indian Ocean.

One striking feature from the observed and modeled signal strength (Figs. 1 and 3) is the negative lobe at 150-200 m depth in the Pacific. The simulation that captured this signal showed it is associated with a thinning of the western Pacific warm pool associated with shoaling of the deeper isotherms, which has also been observed in the Pacific since the 1970s (22).

The major surprise is the N. Indian Ocean, which has rather shallow signal penetration and a sub surface maximum in signal strength. The heat budget for this region (Fig. 4) shows it is the only basin where the ensemble variability includes zero for the net surface heat flux, and where advective warming is the dominant cause of the basin temperature change over the last 60 years in PCM. This result is likely due to the cancellation of GHG warming by sulfate aerosol cooling, a result recently found from direct observations (23). It should be noted that further simulations have shown carbon aerosols also play a role in this effect (24), but are not included in the simulations of this paper. So the warming of this ocean over the past 60 years in the simulation was largely due to changes in advection. Recent observations show a slowing of the shallow meridional circulation cell in the Indian Ocean such that advection from north to south Indian Ocean is reduced, leading to a net warming of the northern Indian ocean (25), a result in accord with the model predictions. Indeed, inspection of the partition of net surface air/sea heat exchange and advection for the various oceans (Fig. 4) shows that in several basins, changes in advection of heat by ocean currents redistribute the heat gained from the anthropogenic forcing, and so is important to determining the structure and evolution of the warming signal in the oceans [cf. (7)].

The normalization by surface area used in Fig. 4 takes out the geometric impact of ocean size on our results. It also makes clear that the southern oceans are absorbing more heat per unit area than are the northern oceans. We suggest that this is again due to the smaller aerosol concentrations over the southern oceans. They do not have the same near-canceling effects observed in the more polluted northern hemisphere (23, 24).

Is PCM unique in being able to capture the complex observed signal? To address this, we repeated the analysis with HadCM3, which has been developed at the Hadley Centre independently of PCM. The four realizations from this

model were the “All” forcings runs, which combined a variety of forcing [GHG, solar, volcanic, aerosols, etc. (26)]. HadCM3’s warming fingerprint (not shown) is little different from PCM’s but we use exclusively PCM’s fingerprint here for consistency. The results from HadCM3 are compared to observations in Fig. 5. Using the HadCM3 fingerprint gives even better agreement (not shown), as one would expect. In any event, Figs. 3 and 5 show that PCM and HadCM3 both do a good job in capturing the evolution and spatial characteristics of the warming signal.

An interesting feature of the above result is that the PCM and HadCM3 are very different models. In the simulations used here their forcings are also rather different. How could they give very similar evolutions of ocean temperature? Whatever the combinations of forcing used by the two modeling groups, the net forcing at the surface of the ocean had to be essentially the same. Inspection of each model’s surface heat flux fields, in so far as possible, shows this to be the case. The details of the atmospheric forcing and climate feedbacks that go into producing that net value do not impact the overall oceanic response. The story may be different in the atmosphere.

It is also important to investigate the influence of the upgraded data set (2), sampling, and model uncertainties on our conclusions. In all our results, we use a sampling strategy that only compares model and observations where observations exist; we do not use the infilled or interpolated data set (11). As a test, however, we repeated the analysis using the infilled data and found it made no difference to the conclusions. More details on these sampling issues are found in (18). We also estimated the impact model errors might have on the results. Multiple models run with the same GHG forcing (CMIP2+ runs available through www-pcmdi.llnl.gov) show a factor of two difference in ocean basin heat content after 80 years of integration (27, 28). We estimated the effect this had in the detection scheme and still found robust detection results above the level of natural variability (18). Therefore the conclusion that the observed ocean warming is due to human influences is robust to major perturbations of both the observed data set and model error.

The implications of our results go far beyond identifying the reasons for ocean warming. First, they show that uncertainties in the models used here are too small to affect the conclusion attributing the historic ocean warming signal to anthropogenic forcings, at least for the temperature driven part of the signal. Second, taking these new results with those obtained in the last few years [e.g., (1, 29–31); see earlier detection studies cited above] leaves little doubt that there is a human-induced signal in the environment. Third, since the historical changes have been well simulated, future changes predicted by these global models are apt to be reasonably good, at least out to, say, 20-30 years into the future. How to

respond to the serious problems posed by these predictions is a question society must decide.

References and Notes

1. IPCC, WG1 Third Assessment Report. J. T. Houghton *et al.* Eds. (2001).
2. S. Levitus, J. Antonov, T. Boyer, *Geophys. Res. Lett.* **32**, L02604, doi:10.1029/2004GL021592 (2005).
3. T. P. Barnett, D. W. Pierce, R. Schnur, *Science* **292**, 270 (2001).
4. S. Levitus *et al.*, *Science* **292**, 267 (2001).
5. B. K. Reichert, R. Schnur, L. Bengtsson, *Geophys. Res. Lett.* **29**, 1525 (2002).
6. J. Hansen *et al.*, *J. Geophys. Res.* **107** (D18), 4347, 10.1029/2001JD001143 (2002).
7. J. M. Gregory, H.T. Banks, P. A. Stott, J. A. Lowe, M. D. Palmer, *Geophys. Res. Lett.* **31** L15312, 10.1029/2004GL020258 (2004).
8. P. R. Gent, G. Danabasoglu, *J. Clim.* **17**, 4058 (2004).
9. W. M. Washington *et al.*, *Clim Dyn.* **16**, 755 (2000).
10. C. Gordon *et al.*, *Clim. Dyn.*, **16**, 147 (2000).
11. Methods are available as supporting material on *Science Online*.
12. Methods are available as supporting material on *Science Online*.
13. G.C. Hegerl *et al.*, *J. Clim.* **9**, 2281 (1996).
14. G. C. Hegerl *et al.*, *Clim. Dyn.* **13**, 613 (1997).
15. M. R. Allen, S.F.B. Tett, *Clim. Dyn.* **15**, 419 (1999).
16. K. Hasselmann, *Clim. Dyn.* **13**, 601 (1997).
17. Methods are available as supporting material on *Science Online*.
18. D. W. Pierce *et al.*, *J. Clim.*, in prep (2005).
19. G. A. Meehl, W. M. Washington, T. M. L. Wigley, J. M. Arblaster, A. Dai, *J. Clim.* **16**, 426 (2003).
20. A. Dai, W. M. Washington, G. A. Meehl, T. W. Bettge, W. G. Strand, *Clim. Change* **62**, 29 (2004).
21. G. Neumann, W. J. Pierson, *Principals of Physical Oceanography* (Prentice-Hall, 1966).
22. M. J. McPhaden, D. Zhang, *Nature* **415**, 603 (2002).
23. V. Ramanathan *et al.*, *J. Geophys. Res.* **106** (D22), 28,371 (2001).
24. V. Ramanathan *et al.*, Proceedings of the National Academy of Sciences, submitted (2005).
25. T. Lee, *Geophys. Res. Lett.* **31**, L18305 (2004).
26. S. F. B. Tett, P. A. Stott, M. R. Allen, W. J. Ingram, J. F. B. Mitchell, *Nature* **399**, 569 (1999).
27. A. P. Sokolov, C. E. Forest, P. H. Stone, *J. Clim.* **16**, 1573 (2003).
28. K. M. AcutaRao *et al.*, *J. Geophys. Res. Oceans*, submitted.
29. B.D. Santer *et al.*, *Science*, **301**, 479 (2003).
30. B.D. Santer *et al.*, *J. Geophys. Res.*, **109**, 10.1029/2004JD005075 (2004).

31. B.D. Santer, J.E. Penner, P.W. Thorne, How well can the observed vertical temperature changes be reconciled with our understanding of the causes of these changes? In: *Temperature Trends in the Lower Atmosphere: Steps for Understanding and Reconciling Differences*. A Report by the U.S. Climate Change Science Plan and the Subcommittee on Global Change Research, Washington, DC (in press).
32. This work is a contribution from the International Detection and Attribution Group funded by the NOAA and DOE through NOAA's CCDD program. We gratefully acknowledge DOE support through grants DE-FG03-01ER63255 to the Scripps Inst of Oceanography and DOE-W-7405-ENG-48 to PCMDI at LLNL. Work at the Hadley Centre was supported by the UK Department for Environment, Food and Rural Affairs under contract PECD 7/12/37 and by the Government Meteorological Research and Development Programme. We especially wish to thank Syd Levitus for his generosity in making his new ocean data set available and to colleagues at NCAR and the Hadley Centre for performing and making available the model runs used in this work. Computer time for the PCM simulations was provided by the NCAR Scientific Computing Division (SCD), the DOE National Energy Research Scientific Computing Center (NERSC), Oak Ridge National Laboratory (ORNL), and the Los Alamos National Laboratory's Advanced Computing Laboratory (ACL). Discussions with Lynne Talley and Russ Davis were helpful in several aspects of the study.

Supporting Online Material

www.sciencemag.org/cgi/content/full/1112418/DC1

Materials and Methods

SOM Text

Figs. S1 and S2

References and Notes

17 March 2005; accepted 12 May 2005

Published online 2 June 2005; 10.1126/science.1112418

Include this information when citing this paper.

Fig. 1. Warming signal strength by ocean and depth. The dots represent the projection of the observed temperature changes onto the model-based pattern of warming. They show substantial basin-to-basin differences in how the oceans have warmed over the past 40 years, although all oceans have experienced net warming over that interval. The horizontal bars represent the \pm two standard deviations limits associated with sampling uncertainty.

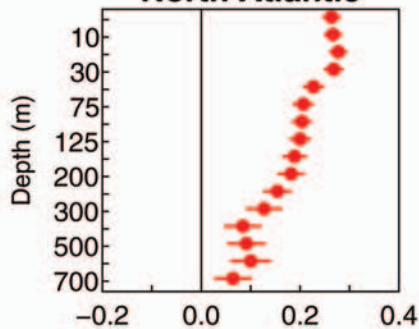
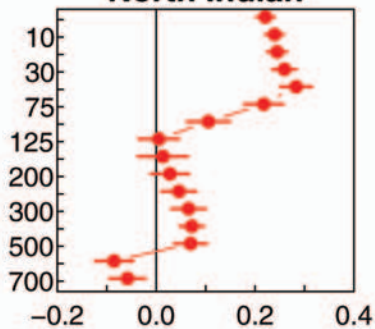
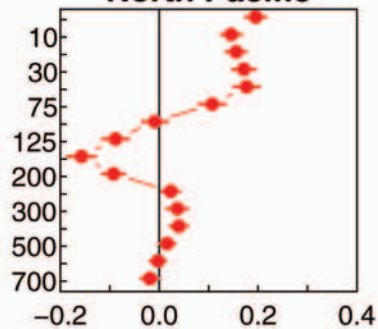
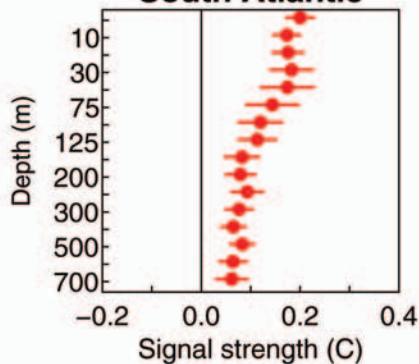
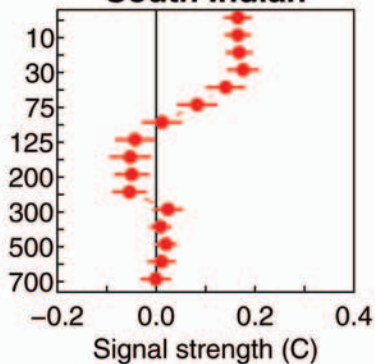
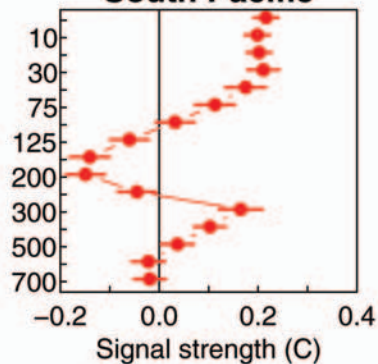
Fig. 2. Multiple realizations from the PCM control run allowed estimation of the probability distribution of signal strength associated with natural internal variability. The

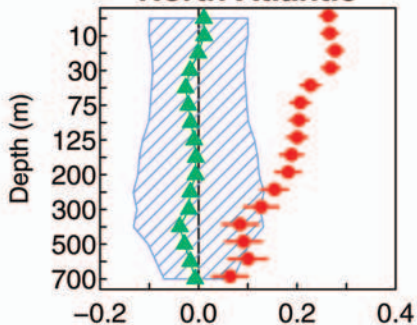
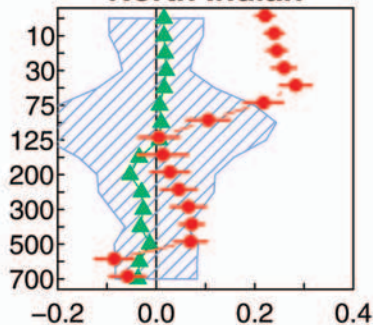
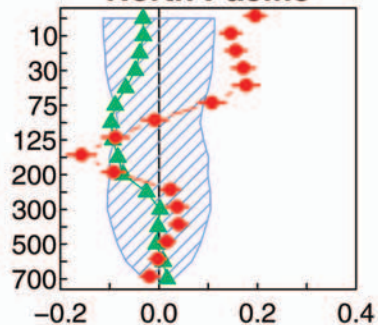
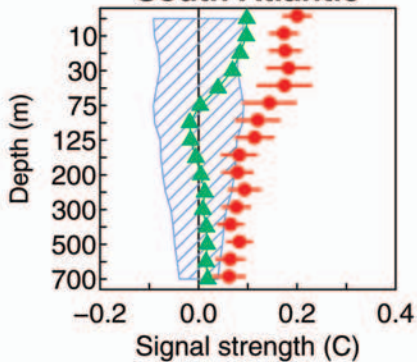
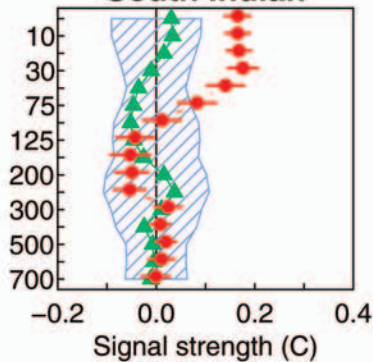
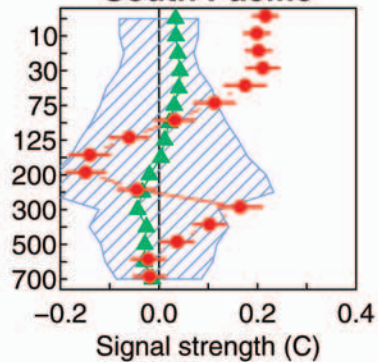
hatched region represents the 90% confidence limits of the natural internal variability signal strength. The observed signal strength (red dots) bears little resemblance to that expected from natural internal variability. The ensemble averaged strength of the warming signal in four runs forced by observed solar and volcanic variability (green triangles) is also shown. There is no agreement between the two. The solar+volcanic signals are generally indistinguishable from those expected from natural internal variability alone on the time and space scales used in this study.

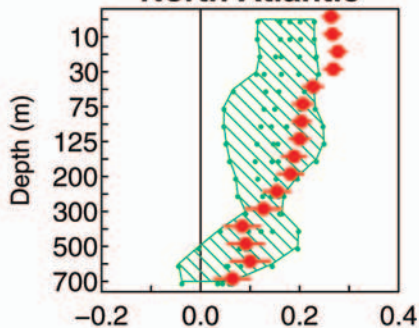
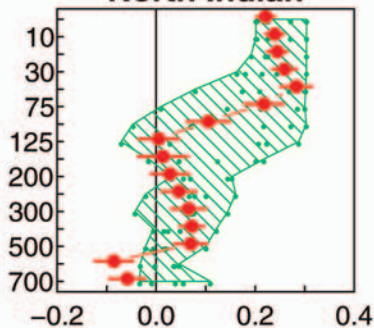
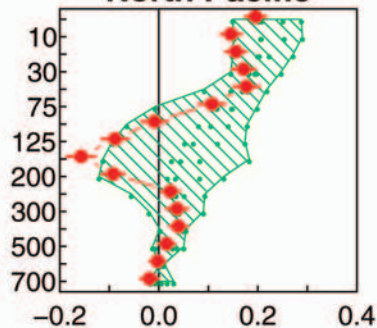
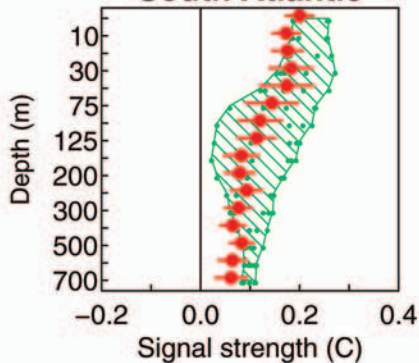
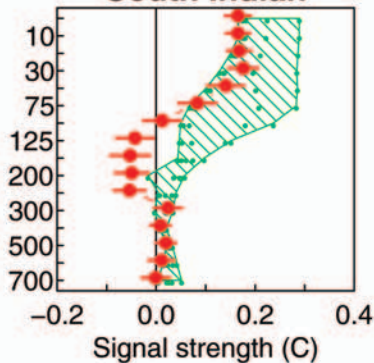
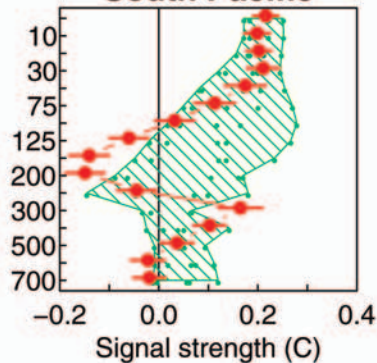
Fig. 3. Anthropogenic forcing signal strength (green hatched region) compared to that obtained from the observations (red dots). There is excellent agreement at most depths in all oceans. The hatched region shows the range of the signal strength estimates from five different realizations of identically forced simulation with the PCM, while the smaller green dots within the region are the individual realizations.

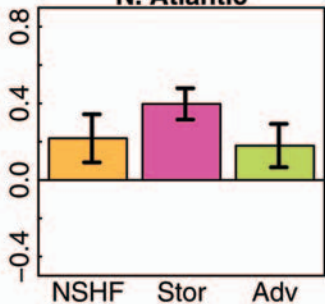
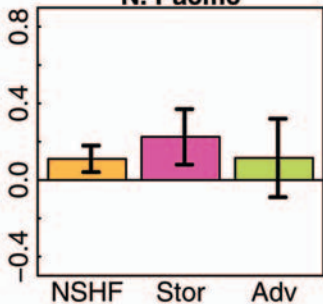
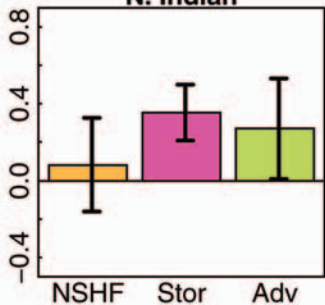
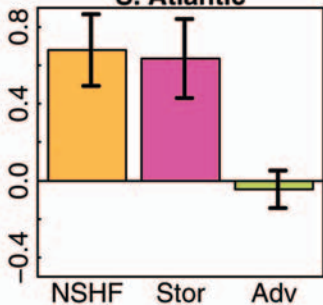
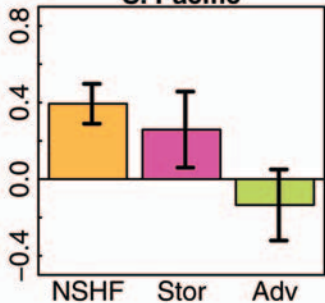
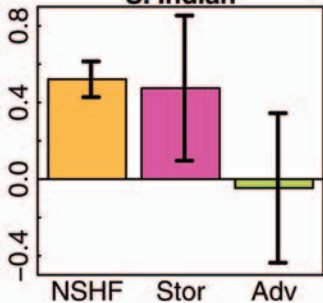
Fig. 4. Gross heat budget by ocean showing the important role heat advection by ocean currents plays in the anthropogenic warming of the world's oceans. The PCM's net ocean surface heat flux averaged over 1940-1999 is shown by the 'NSHF' bars, the modeled changes in ocean basin heat storage by the 'Stor' bars, and the advection of heat by ocean currents needed to close the heat budget by the 'Adv' bars. The latter was obtained as a residual from the first two estimates. The uncertainty bars indicate \pm one standard deviation based on the ensemble spread. Note the actual energy change (joules) over the time period has been normalized by surface area of respective oceans to give the average heating rate in W/m^2 . This normalization makes it appear that the net advection over the globe is nonzero, a condition that vanishes using the area-weighted fluxes.

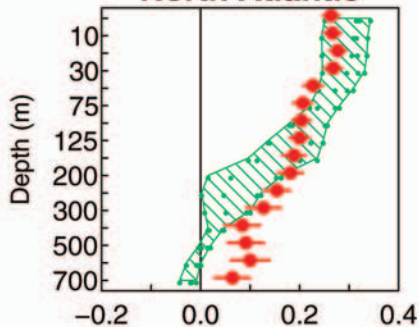
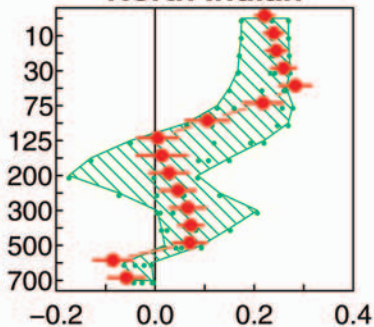
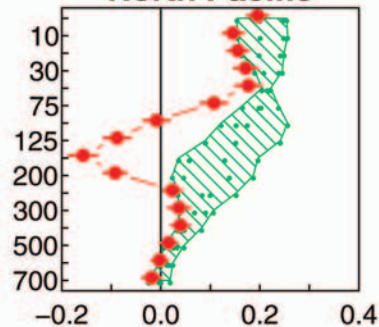
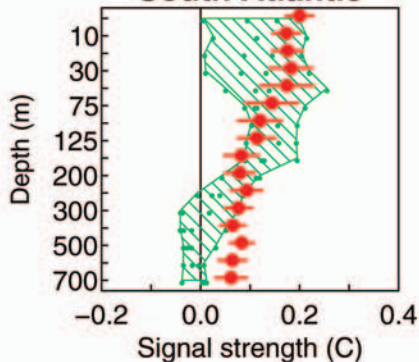
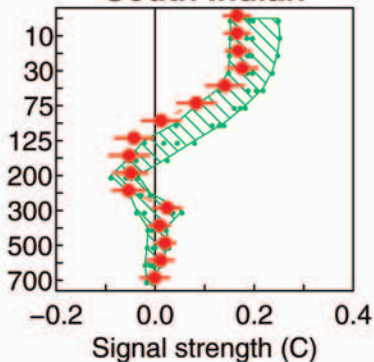
Fig. 5. Comparison of the model predicted anthropogenic signals between HadCM3 and observations for the oceans. The format is described in Fig. 3. Comparison of Figs. 3 and 5 clearly shows both models capture the main structure of the signal in the observations. These figures were derived by using the warming signal defined by PCM as the basis set to allow a consistent comparison.

North Atlantic**North Indian****North Pacific****South Atlantic****South Indian****South Pacific**

North Atlantic**North Indian****North Pacific****South Atlantic****South Indian****South Pacific**

North Atlantic**North Indian****North Pacific****South Atlantic****South Indian****South Pacific**

N. Atlantic**N. Pacific****N. Indian****S. Atlantic****S. Pacific****S. Indian**

North Atlantic**North Indian****North Pacific****South Atlantic****South Indian****South Pacific**